The effect of contact load on CoCrMo wear and the formation and retention of tribofilms

M.A. Wimmer [a,*], M.P. Laurent [a], M.T. Mathew [a], C. Nagelli [a], Y. Liao [b], L.D. Marks [b], J.J. Jacobs [a], A. Fischer [a,c]

[a] Rush University Medical Center, Chicago, IL, USA
[b] Department of Material Science, Northwestern University, Evanston, IL, USA
[c] Materials Science and Engineering, University of Duisburg-Essen, Duisburg, Germany

ARTICLE INFO

ABSTRACT

Tribochemical reactions in a protein lubricated metal-on-metal (MoM) sliding contact may play a significant role for its wear performance. Such reactions lead to the formation of a carbonaceous 'tribofilm', which can act as a protective layer against corrosion and wear. The purpose of this study was to determine the effect of contact load on wear and the formation and retention of tribofilms.

Wear tests were performed in a custom-made ball-on-flat testing apparatus that incorporated an electrochemical cell. A ceramic ball was used to articulate against low-carbon wrought CoCrMo alloy pins in bovine serum. Using a range of contact loads at a single potentiostatic condition (close to free potential), weight loss and changes in surface properties were evaluated.

We determined that wear was influenced by the loading condition. As expected, wear increased with load, but the association between applied load and measured weight loss was not linear. In the intermediate load region, in the range of 32–48 N ($\sim$58–80 MPa), there was more than an order of magnitude drop in the wear per unit load, and the wear versus load data suggested an inflexion point at 49 N. Regression analyses yielded a cubic model ($R^2=0.991$; $p=0.0002$), where the cubic term, which represents the inflexion, was highly significant ($p=0.0021$). This model is supported by the observations that the minimum in the friction versus load curve is at 52 N and the highest relative increase in polarization resistance occurred at 49 N. Scanning electron microscopy and Raman spectroscopy indicated the absence of a tribofilm for the low and within the contact area of the high load cases. Synergistic interactions of wear and corrosion seem to play an important role.

© 2015 Elsevier B.V. All rights reserved.

1. Introduction

Until recently approximately one third of the more than 300,000 annually performed hip arthroplasties in the United States were made of self-mating cobalt–chromium (CoCr) alloy bearing surfaces [1]. A steadily growing patient population, being younger of age at the time of surgery and having increased activity demands, did raise the proportion of so-called 'metal-on-metal' (MoM) joints in hip arthroplasty during the last decade. Unfortunately, failure rates of some of these metal-on-metal (MoM) devices have been reportedly high [2–5], and many of these failures have been attributed to adverse local tissue reactions [6–8]. The high failure rates and the – in some cases – drastic soft tissue reactions are unexpected since MoM hip arthroplasty has been in clinical use since the 1960s, and has often been cited as a low wearing alternative to conventional polyethylene. Particularly, the

so-called second generation of MoM devices with a 'small' 28 mm diameter CoCr balls and matching, hemispherical cups functioned reasonably well over the years with good survival rates [5].

Several risk factors for high wear of large diameter MoM bearings have been identified, e.g. steep inclination and high version angles [9], low coverage of the head with cup [10], edge loading [11], female sex [12], etc. the mechanism of failure is not well understood. Here, we speculate and provide evidence that this could be related to the presence or absence of tribofilms. A 'tribofilm' is a carbonaceous layer or film ('tribofilm') that forms on the surfaces of MoM components [13–17]. We have recently reported that the film contains graphitic material [18], although this has yet to be independently confirmed [17]. Still, the film may act as a boundary lubricant in the absence of full fluid film lubrication due to its proteinaceous origin [13]. During tribocorrosive testing, the presence of a tribofilm reduced friction and wear, as well as increased corrosion resistance [19,20]. Tribofilms therefore seem critical to reducing wear and corrosion in MoM bearings, and it is of interest to determine what factors influence their

* Corresponding author. Tel.: +1 312 9422789; fax: +1 312 9422101.
E-mail address: markus_a_wimmer@rush.edu (M.A. Wimmer).

Table 1
Elemental composition of low-carbon CoCrMo alloy (manufacturer data).

Element	C	Co	Cr	Mo	Si	Mn	Al
wt%	0.034	64.96	27.56	5.70	0.38	0.60	< 0.02

Table 2
Chemical composition of BCS solution.

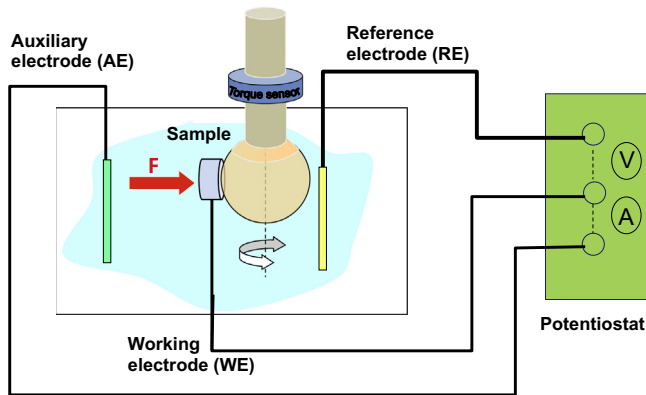| NaCl (g/L)	EDTA (g/L)	Tris (g/L)	Protein (g/L)
9	0.2	27	30

Fig. 1. Schematic drawing of the experimental set-up. A 28 mm diameter alumina ball articulates against the flat face side of a CoCrMo pin within a container filled with bovine serum lubricant. The sample is connected to a potentiostat. A graphite rod and a standard calomel electrode (SCE) serve as auxiliary and reference electrode in this 3-electrode set-up. (Note: for clarity, the UHMWPE support bearing counterbalancing the applied force through the pin is not shown. Further technical details of the apparatus are described in [38]).

formation and effect on wear. Contact load (or the resulting stress) is an inherent variable tied to the previously discussed risk factors. For example, edge loading will increase the contact stress on certain areas of the implants, while a tight clearance and a large coverage arc of ball and cup may lower it. The purpose of the study was therefore to determine the effect of contact load on CoCrMo wear and the tribofilm formation and retention during articulation. A pin-on-ball test configuration was used, in which an alumina ball articulated against the flat face of a CoCrMo pin. We hypothesized that due to the occurrence of load dependent tribochemical reactions, wear of the CoCrMo alloy will not increase linearly with normal load. Regression modeling was used to detect such deviations from linearity.

2. Materials and methods

2.1. Samples

Cylindrical pins from low-carbon CoCrMo wrought alloy (Table 1) according to ASTM Standard F1537 [21] (ATI Allvac, USA) were machined to dimensions of 12 mm in diameter and 7 mm in length. The front end of the pins were mechanically polished to a mirror finish ($R_a \leq 10$ nm) using traditional metallographic methods. Samples were then cleaned in an ultrasonic bath, initially in de-ionized water and then in 70% isopropanol for 10 min each. Finally, surfaces were dried using a blow dryer in clean air.

2.2. Tribocorrosion testing

Tribocorrosion tests were conducted in a custom-made apparatus, where an alumina ball of 28 mm diameter (Biolox Forte, CeramTec GmbH, Plochingen, Germany) articulated against the flat front face of the pin (Fig. 1). The ceramic ball was used to electrically isolate the metal pin from the countersurface. Analogous to corrosion tests, a three-electrode system of working,

auxiliary and reference electrode was used and consisted of the exposed CoCrMo pin surface (1.13 cm^2), graphite rod and calomel electrode (SCE). A total volume of 150 ml of new born bovine calf serum (BCS), diluted to 30 g/l protein content to simulate synovial fluid (Table 2), was used as the electrolyte and lubricant. During testing it was maintained at 37 °C and pH 7.6. The ball was pressed against the pin and oscillated around an axis parallel to the pin's surface with $\pm$ 15° (sweep of 30°) at 1 Hz for a total of 1800 cycles. Friction was measured using a torque sensor (TRT-200, Transducer Technique, Temecula, CA, USA) (Fig. 1). Forces ranging from 8 N to 64 N with an interval increment of 8 N were chosen as contact loads. Each contact condition was repeated for $n=5$ pins, and all tests were conducted under potentiostatic conditions with the pin at a fixed potential of -345 mV vs. SCE, which is close to the free corrosion potential (-325 mV vs. SCE) of CoCrMo as identified in earlier corrosion tests according to ASTM standard G61 [20,22].

The tribocorrosion protocol consisted of three major steps: (1) an initial stabilization period where a potential of -900 mV (vs. SCE) was applied for 10 min across the sample's surface to cathodically clean the surface, followed by a period with OCP to stabilize the system; (2) a tribological testing period where the ceramic ball articulated against the CoCrMo pin under fixed potential; and (3) a final stabilization period where the OCP was monitored to again electrochemically stabilize the system after tribological testing. Fig. 2 provides an overview of the testing procedure. Electrochemical impedance spectroscopy (EIS) measurements were performed immediately before and after sliding, i.e., step (2). A potentiostat (G 700, Gamry Inc., USA) was used to carry out the measurements within a frequency range of 100 kHz–0.005 Hz and an AC sine wave amplitude of 10 mV. Runs that that showed erratic behavior in the Nyquist and Bode plots, i.e., irregular excursions from the expected monotonic shape and missing points, were excluded, because such behavior makes the data unsuitable for modeling. The remaining runs were modeled with Randle's simple equivalent circuit composed of electrolyte resistances (R_s) in series with a constant phase element (CPE) and in parallel with the polarization resistance (R_p) (ZView software, Scribner Associates, USA). Only fittings with chi-square < 0.01 were accepted. From each loading group the run with the lowest chi-square was chosen, and the polarization resistance, R_p, before and after sliding was determined. Changes in polarization resistance are expressed normalized to the starting condition (R_p-after/ R_p -before).

2.3. Calculation of friction coefficient

In order to determine the friction coefficient (COF) and compare it to contact load, material loss and surface condition, the frictional torque of the last 300 cycles has been averaged for each sample. Then, the COF was calculated by dividing the frictional torque by the ball radius (14 mm) and subtracting 0.04 to account for the UHMWPE bearing support, which counterbalances the applied normal force. The value of 0.04 has been determined in earlier experiments using UHMWPE for both sample and support bearing in bovine serum lubricant.

2.4. Measurement of material loss

The wear scar volume was determined using microtopographical measurements. From each wear scar, 3-D profiles were generated using white light interferometry (NewView 6300, Zygo Corp., USA).
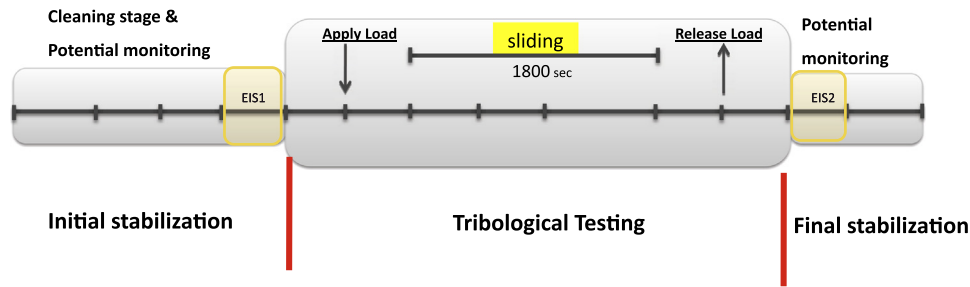
Fig. 2. Overview of the tribocorrosion protocol consisting of three major periods: initial stabilization, tribological testing (sliding), and final stabilization period. The EIS windows determine when electrochemical impedance spectroscopy is performed.

The lost volume was then calculated and translated into mass loss by taking the density of 8.462 g/cm^3 of the CoCrMo alloy (manufacturer data) into account. After completion of the experiments, approximately 1 ml of electrolyte per sample was transferred into quartz vessels together with 2 mL nitric acid (60%) and 5 mL H_2O and digested in the microwave. The cobalt and chromium content was then determined using mass spectrometry techniques. The detection limits were 40 ppb for cobalt and 10 ppb for chromium.

2.5. Synergistic interaction

The synergistic interaction between wear and corrosion was studied by using the method according to Stack and Abdulrahman [23]. Briefly, this method uses the weight loss governed by corrosion (K_c) and contrasts it against the weight loss due to wear (K_w) in form of the ratio K_c/K_w.

The total weight loss (K_{wc}), inferred from white light interferometry, was expressed as the sum of the weight loss due to wear (K_w) and due to corrosion (K_c):

$$K_{wc} = K_w + K_c \tag{1}$$

K_c was estimated using Faraday's Law [24]:

$$K_c = \frac{M \times i \times t}{n \times F} \tag{2}$$

and

$$i \times t = Q \tag{3}$$

where 'M' is the atomic mass of the material or equivalent weight in g/mol, 'i' is the total current density in A/cm^2, 't' is the total exposure time in seconds, 'n' is the number of electrons involved in the corrosion process which can be 2^+, and 3^+ (for the simplicity $n=2$ is assumed for this study), 'F' is the Faraday's constant (96,500 C/mol^{-1}), and 'Q' is the charge passed through the working electrode in coulombs. In order to classify the dominant degradation mechanism, criteria established by Stack and Abdulrahman [23] were used. Based on the ratio of K_c/K_w the following classification groups are considered:

$$K_c/K_w < 0.1 \text{ Wear} \tag{4}$$

$$0.1 \leq K_c/K_w < 1 \text{ Wear} - \text{corrosion} \tag{5}$$

$$1 \leq K_c/K_w < 10 \text{ Corrosion} - \text{wear} \tag{6}$$

$$K_c/K_w \geq 10 \text{ Corrosion} \tag{7}$$

2.6. Surface analyses

After testing, the samples underwent the same cleaning procedure as was used for sample preparation using deionized water and isopropanol. Every sample was characterized by white light interferometry for surface topography and scanning electron microscopy (SEM) (JSM 5600, JOEL Co., Japan) for surface appearance. Observed surface layers were characterized using energy dispersive x-ray spectroscopy (EDS). The presence or absence of carbonaceous tribolayers as suggested by SEM and EDS was further investigated using confocal Raman spectroscopy with excitation radiation of an Ar–Kr 514.5 nm gas laser at ∼10 mW. Spectra were recorded in the range of 1100–1900 cm^{-1}. Typical collection times were 30 s and the accumulation of several measurements per sample are reported. In order to discriminate adhering proteins from carbonaceous tribofilms, the obtained spectra were fitted using the D and G lines of graphitic carbon as described earlier [18].

2.7. Statistics

The wear volume versus load data was evaluated using polynomial regression (Design Expert Version 9, Stat-Ease, Inc., Minneapolis, Minnesota). This approach permitted the statistical quantification of the inflexion region in the data, evident by inspection. The data was log-transformed for variance stabilization, and model selection was effected with a backward regression procedure allowing up to a sixth power term for the load. Regression analyses were also performed to investigate relationships of contact load with the friction coefficient and of wear volume with metal ion data. Probability p-values and coefficient of determination R^2 values are reported as a measure of the strength of the models. Standard errors, rather than standard deviations, were reported for the means, given we are interested in comparing the means of the output variables (wear volume, COF, Rp, etc.) across loading groups. The one-sample t-test was used to test the hypothesis that the mean of the group's synergistic ratio is equal to 0.1.

3. Results

All load levels generated approximately circular wear scars where the ratio of largest to smallest diameter was 1.19 ± 0.11 (Fig. 3). The final, technical contact stresses ranged from approximately 30–100 MPa, depending on load and wear scar area (Table 3).

The friction coefficient was highest at the lowest load, ranging from 0.37 at 8 N to 0.22 at 48 N (Table 4). The magnitude of the friction values suggests that the ceramic ball–metal pin couple was operating under boundary lubrication at all the loads, which is expected based on the geometry of the bearing couple. Regression analysis indicated that the friction data was best fitted with a second order polynomial function ($R^2=0.739$; $p=0.035$), which predicts that the friction minimum occurs at 52 N (Fig. 4).

As expected, wear scar volume and calculated material loss increased with load (Table 5). The wear volume correlated significantly with the measured metal content levels in the electrolyte
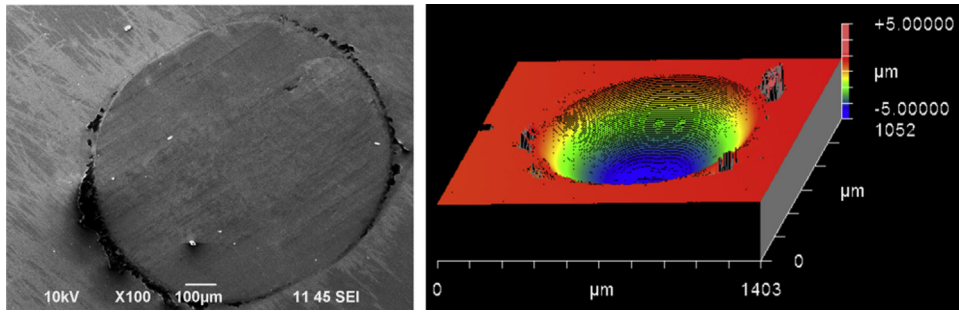
Fig. 3. Wear scars as seen by SEM and White light interferometry.

Table 3
Applied contact load and final (technical) contact stress. Data in mean ($\pm$ SEM).

Load [N]	8	16	24	32	40	48	56	64
Stress [MPa]	33.1 (1.7)	43.4 (2.2)	47.4 (1.7)	57.5 (1.7)	69.3 (2.2)	80.0 (1.7)	87.2 (2.6)	101.0 (2.3)

Table 4
Applied contact load and friction coefficient. Data in mean ($\pm$ SEM).

Load [N]	8	16	24	32	40	48	56	64
COF [dimensionless]	0.37 (0.06)	0.27 (0.05)	0.32 (0.04)	0.28 (0.05)	0.23 (0.01)	0.22 (0.03)	0.22 (0.02)	0.26 (0.02)

($p=0.001$; $R^2=0.336$). However, the regression line did not intercept at 0 ppb but at 79 ppb.

The CoCrMo wear volume did not increase linearly with load, exhibiting instead a pronounced inflexion or leveling region between 32 N and 56 N (Fig. 5). Regression analysis performed on the average wear values versus load yielded a robust cubic model that closely follows the data ($R^2=0.991$, $p=0.0002$, Fig. 5), where the cubic term, which represents the inflexion, was highly significant ($p=0.0021$). It may thus be reasonably concluded that the wear leveling is real. According to this model, the slope decreases from 3.2E-5 mm^3/N at 16 N to a minimum of -4.3E-6 mm^3/N at 42 N, then increasing to 1.5E-5 mm^3/N at 56 N and 6.1E-5 mm^3/N at 64 N.

Calculated values of K_c and K_w are presented in Table 6. The synergistic ratio K_c/K_w was above 0.1 in most cases (Fig. 6), indicating a relevant contribution of corrosion to total material loss. Only for the 8 and 64 N loading groups was it significantly below 0.1 ($p=0.004$ and 0.045, respectively), suggesting that mechanical wear was dominant in the lowest and highest load level groups.

SEM examination of the worn surfaces suggested abrasion as a major wear mechanism for this wear couple. Scratches and grooves were seen on all samples and for all load levels (Fig. 7a–c). Dark tribofilms with a characteristic carbon-peak in the EDS spectra were also seen on most samples, but were absent in the 8 N load cases (Fig. 7a and b). For the 64 N loading group, tribofilms were less pronounced in the center of the wear scars, and the surfaces were clearly more damaged (Fig. 7c). Raman analysis (Fig. 8) also revealed the occurrence of tribofilms for all but the 8 N load group. Interestingly, for the 64 N load group the Raman signal was not always very strong and sometimes absent within certain areas of the wear scar. Such findings were mirrored by the results of the EIS analysis, where the polarization resistance typically increased from before to after testing (Fig. 9), indicating a change in electrochemical surface film properties. The change was highest for the 40 N and 56 N load cases and regression analysis predicted the maximum R_p at 49 N (cubic model, $R^2=0.846$, $p=0.042$, Fig. 5), but absent for the 8 N level suggesting
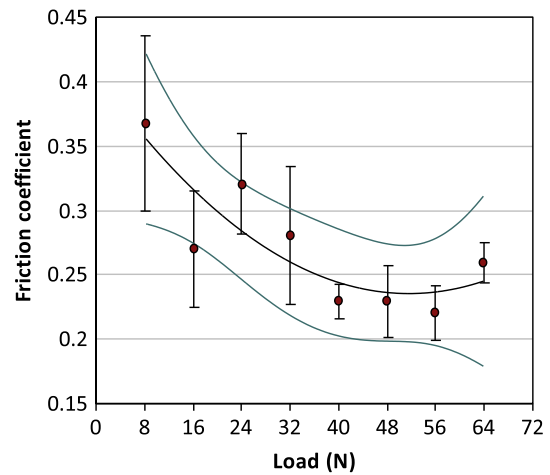

Fig. 4. Resulting friction coefficient (last 300 cycles of experiment) as a function of load. The results of five samples per load level are graphically displayed as mean $\pm$ SEM. The fitted regression line is shown flanked by the 95% confidence interval bands. It has a minimum at 52 N.

that the original chromium oxide film may have stayed intact for the lowest load level.

4. Discussion

As hypothesized, the volumetric wear of the CoCrMo pins did not increase linearly with the applied normal load. This finding is consistent with the formation of a load-dependent tribofilm, which changes the wear mechanism in certain loading regimes. Interestingly, the amount wear was quite insensitive to load within a certain window of normal load. This finding underscores the importance of tribochemical reactions, which are capable of limiting wear particle and ion release by forming a protective surface film. The results also suggest that a certain minimum load

Table 5
Applied contact load and wear scar volume. Data in mean ($\pm$ SEM).

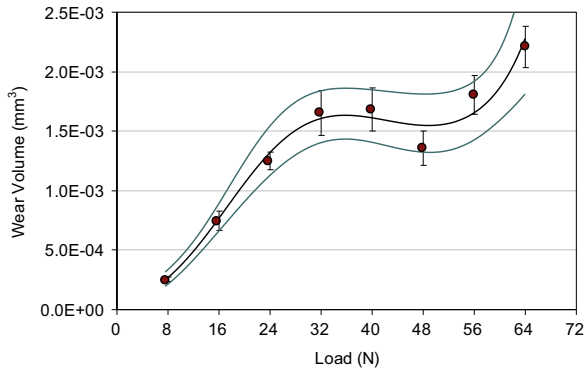| Load [N]	8	16	24	32	40	48	56	64
Volume [$\times 10^{-3}$ mm^3]	0.20 (0.05)	0.74 (0.17)	1.25 (0.08)	1.66 (0.19)	1.68 (0.13)	1.36 (0.12)	1.80 (0.14)	2.21 (0.18)

Fig. 5. The total volume loss of CoCrMo as a function of load. Each point is the mean $\pm$ SEM from five pins, except at 8 N, where $n=4$ due to an outlier. The fitted cubic regression line is shown flanked by the 95% confidence interval bands. It has a minimum at 49 N.

Fig. 6. The synergistic ratio K_c/K_w shown for various load levels. There is a change in classification for the lowest and the highest load level.

is necessary to initiate tribofilm formation. Once formed, the tribofilm is only stable up to a maximum load before it is either being abraded or pushed out of the contact area.

All the samples showed signs of abrasion, which is a dominant wear mechanism in MoM joints [13]. Since the tests were performed with a low-carbon CoCrMo alloy, micro-cracking – a submechanism of abrasion – can be ruled out. Indeed, no indentations on the surfaces were visible, supporting this assumption. Hence, micro-cutting and micro-plowing prevail as abrasive mechanisms during this short-term experiment. In parallel, tribochemical reactions are taking place. Those include the dissolution of the metal alloy, as evidenced by the increased current flow during articulation of pin and ball. The importance of wear-accelerated corrosion, or 'tribocorrosion', of passive metals in aqueous media was described nearly two decades ago [25] and has been intensely applied in studies involving CoCrMo-alloys [26–31]. All these studies highlight the importance of tribocorrosion in the degradation of CoCrMo alloy. One of our own studies concluded that the occurrence of proteins directly affects the synergism of wear and corrosion in the tribocontact [32]. The release of molybdenum(VI)-ions during tribocorrosion might be responsible for the formation of a proteinaceous layer on the surface [33], which then undergoes mechanical mixing under the applied tribological stresses to form a tribofilm [34,35]. The results of this study suggest that the presence of a tribofilm diminishes the load sensitivity of wear and leads to a constant rate of material loss over a substantial range of applied contact stress.

It appears that a certain minimum load is necessary to initiate tribochemical reactions and film generation. The exact mechanism is presently unknown, but contact stresses below 40 MPa might be insufficient to remove the protecting chromium oxide layer (inherent passive film) and prevent the release of a sufficient amount of molybdenum ions for film formation. Another possibility is that too little energy is introduced into the system at low loads in order to facilitate direct adherence of a proteinaceous layer through an unknown mechanism [36] and/or mechanical mixing of the film with the alloy. Recent research suggests that the necessary vortices for mechanical mixing can be generated by severe plastic deformation and overfolding of the alloy at microstructural obstacles [37]. Without mechanical mixing, the
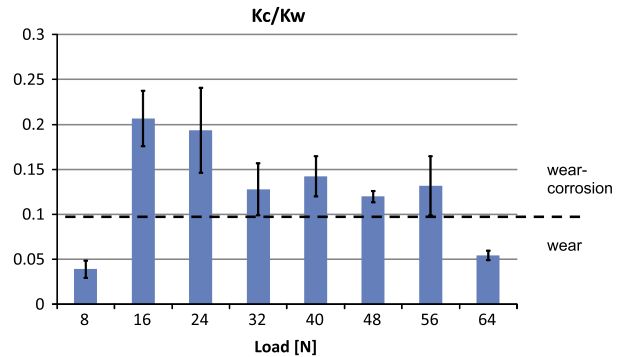
adhering protein film may be easily removed from the contact region without tribological benefits. At too high contact stresses, on the other hand, as seen here at loads exceeding 90–100 MPa, the tribofilm may be abraded or squeezed out of the contact and never reach sufficient stability to protect the surface.

In order to identify wear and corrosion, complementary strategies were used. It was shown that wear is *not* proportional to normal load times sliding distance and that hence the Archard equation does not apply. This nonlinearity is consistent with the occurrence of a tribofilm, which changes the surface properties of the two bodies in contact. In addition, the observation is supported by the evolution of the synergistic ratio (K_c/K_w), the change in polarization resistance, and qualitative findings by means of SEM and Raman spectroscopy. Weight loss was determined by volumetric methods and verified by determining the metal content in the surrounding medium. Interestingly, the correlation of metal content with volumetric material loss produced a positive intercept on the abscissa, suggesting that even in the absence of a wear scar, metal release occurs. It is known that the disruption of the oxide film can lead to a potential difference between the wear area and the surrounding metal [25], which facilitate corrosion on the surface surrounding the contact area.

A limitation of this study was the use of an alumina ball as a counterbody to electrochemically isolate the CoCrMo alloy. This was necessary to keep the CoCrMo alloy under controlled electrochemical conditions during the tribocorrosion testing. A second limitation is the use of a ball-on-flat contact configuration instead of the regular hip joint contact geometry. This configuration had the advantage of easy sample preparation; however, such configuration leads to diminishing contact stresses during the test. Still, using a flat counterface, CoCrMo pins could be polished to mirror finish using typical metallurgical equipment. In addition, the flat surface produced small, well defined wear scars amenable to precise wear volume determinations and to detailed surface examination. A third limitation is the relatively short duration of each experiment. More cycles per test would have generated higher material loss and thus more accurate wear readings. However, the execution of 1800 cycles per test was chosen for consistency with earlier analyses [29].

Table 6
Distribution of total weight loss into corrosion (K_c) and mechanical wear (K_w) terms. Data in mean ($\pm$ SEM).

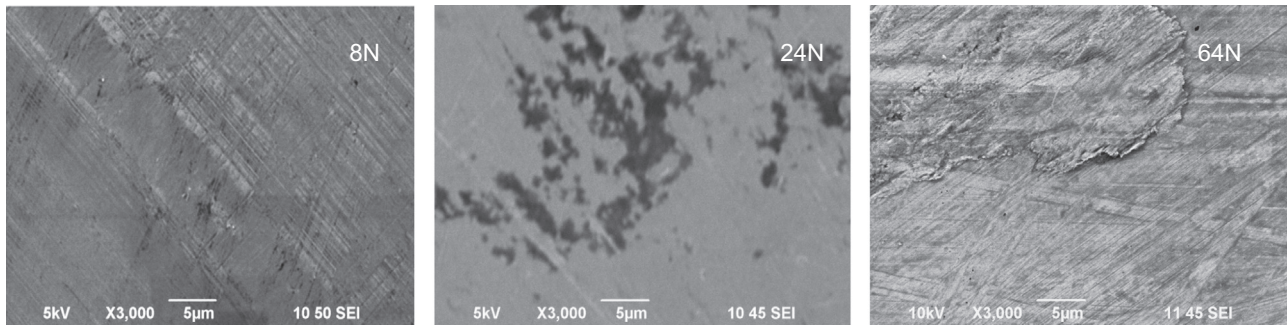| Load [N]	8	16	24	32	40	48	56	64
K_c [µg]	0.08 (0.01)	1.17 (0.16)	1.72 (0.41)	1.60 (0.31)	1.92 (0.28)	1.29 (0.08)	2.03 (0.40)	1.10 (0.12)
K_w [µg]	1.71 (0.39)	5.17 (1.35)	8.86 (0.47)	12.46 (1.83)	11.76 (1.23)	10.10 (1.17)	12.56 (1.36)	17.56 (1.77)

Fig. 7. SEM analysis. The 8 N samples showed only slight scratching on the surfaces. Higher load levels caused the appearance of tribofilms, as shown exemplified for a 24 N sample. The samples of the highest load category were most damaged.
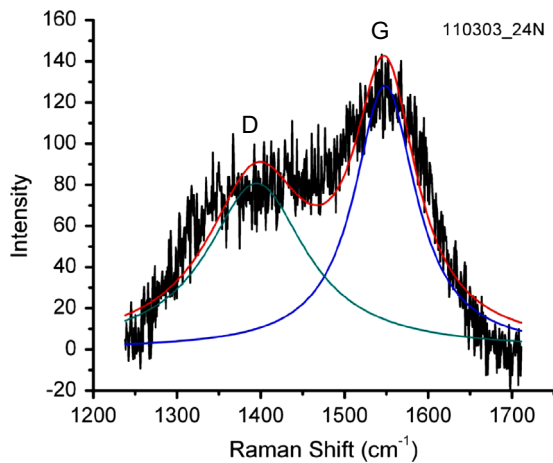

Fig. 8. Raman spectrum of tribofilm on a 24 N sample. The D (cyan) and G (blue) lines of graphitic carbon are shown. The tribofilm signal is fitted by two Gaussian peaks (red). (For interpretation of the references to color in this figure legend, the reader is referred to the web version of this article.)

Fig. 9. Polarization resistance after sliding normalized to the resistance before sliding. The 40 and 48 N load levels generated a 2.5 to 3-fold increase in polarization resistance compared with the starting condition. Higher loads caused a diminished change in film resistance. The regression line is shown flanked by the 95% confidence interval bands. It has a maximum at 49 N.

5. Conclusion

In conclusion, our study suggests that loading conditions influence tribofilm formation. Wear and corrosion synergistic analysis indicates the presence of a specific load range (a window) that promotes tribolayer formation. Outside this range, tribolayer formation appears to be adversely affected. This study suggests that the performance of MoM joints could be improved by designing them to maximize the time that the bearing contact stresses are within the range that favors tribofilm formation. It also suggests that some patients with a MoM prosthesis could benefit from regulation of activities to keep the bearing load below the high wear threshold as much as possible. Because the real contact area is smaller than the nominal one used in this study, further experiments and computer simulations will be carried out to evaluate the range of local pressure values under which the tribofilm is formed and stabilized.
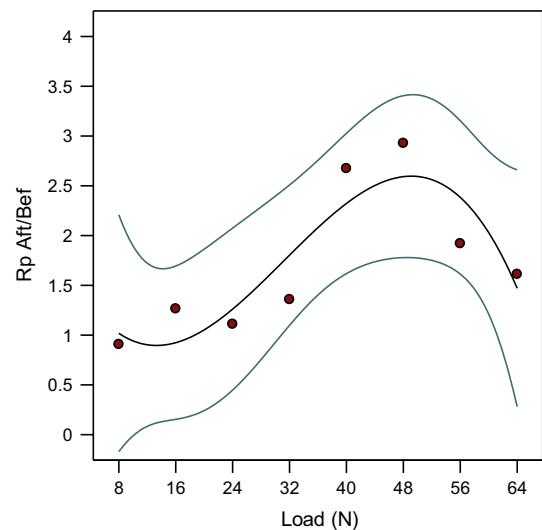
References

[1] S.M. Kurtz, K.L. Ong, E. Lau, A.S. Greenwald, K. Bozic, Prevalence of metal-on-metal bearings in the United States, in: S.M. Kurtz, A.S. Greenwald, W.M. Mihalko, J.E. Lemons (Eds.), Metal-on-Metal Total Hip Replacement Devices, ASTM International, West Conshohocken, 2013, pp. 3–18, STP 1560.

[2] K.J. Bozic, S. Kurtz, E. Lau, K. Ong, V. Chiu, T.P. Vail, H.E. Rubash, D.J. Berry, The epidemiology of bearing surface usage in total hip arthroplasty in the United States, J. Bone Joint Surg. Am. 91 (2009) 1614–1620.

[3] D.J. Langton, S.S. Jameson, T.J. Joyce, J.N. Gandhi, R. Sidaginamale, P. Mereddy, J. Lord, A.V. Nargol, Accelerating failure rate of the ASR total hip replacement, J. Bone Joint Surg. Br. 93 (2011) 1011–1016.

[4] R. Underwood, A. Matthies, P. Cann, J.A. Skinner, A.J. Hart, A comparison of explanted articular surface replacement and birmingham hip resurfacing components, J. Bone Joint Surg. Br. 93 (2011) 1169–1177.

[5] W.M. Mihalko, M.A. Wimmer, C.A. Pacione, M.P. Laurent, R.F. Murphy, C. Rider, How have alternative bearings and modularity affected revision rates in total hip arthroplasty? Clin. Orthop. Relat. Res. (2014).

[6] H.G. Willert, G.H. Buchhorn, A. Fayyazi, R. Flury, M. Windler, G. Koster, C.H. Lohmann, Metal-on-metal bearings and hypersensitivity in patients with artificial hip joints. A clinical and histomorphological study, J. Bone Joint Surg. Am. 87 (2005) 28–36.

[7] G. Mabilleau, Y.M. Kwon, H. Pandit, D.W. Murray, A. Sabokbar, Metal-on-metal hip resurfacing arthroplasty: a review of preprosthetic biological reactions, Acta Orthop. 76 (2008) 734–747.

[8] Y.M. Kwon, S. Glyn-Jones, D.J. Simpson, A. Kamali, P. McLardy-Smith, H.S. Gill, D.W. Murray, Analysis of wear of retrieved metal-on-metal hip resurfacing implants revised due to pseudotumours, J. Bone Joint Surg. Br. 92 (2010) 356–361.

[9] M.M. Morlock, N. Bishop, J. Zustin, M. Hahn, w. Ruther, M. Amling, Modes of implant failure after hip resurfacing: morphological and wear analysis of 267 retrieval specimens, J. Bone Joint Surg. Am. 3 (2008) 89–95.

[10] R. De Haan, C. Pattyn, H.S. Gill, D.W. Murray, P.A. Campbell, K. De Smet, Correlation between inclination of the acetabular component and metal ion levels in metal-on-metal hip resurfacing replacement, J. Bone Joint Surg. Br. 90 (2008) 1291–1297.

[11] A.J. Hart, S. Muirhead-Allwood, M. Porter, A. Matthies, K. Ilo, P. Maggiore, R. Underwood, P. Cann, J. Cobb, J.A. Skinner, Which factors determine the wear rate of large-diameter metal-on-metal hip replacements? Multivariate analysis of two hundred and seventy-six components, J. Bone Joint Surg. Am. 95 (2013) 678–685.

[12] M.J. Latteier, K.R. Berend, A.V. Lombardi Jr., A.F. Ajluni, B.E. Seng, J.B. Adams, Gender is a significant factor for failure of metal-on-metal total hip arthroplasty, J. Arthroplasty 26 (2011) 19–23.

[13] M.A. Wimmer, C. Sprecher, R. Hauert, G. Tager, F. Fischer, Tribochemical reaction on metal-on-metal hip joint bearings – a comparison between in-vitro and in-vivo results, Wear 255 (2003) 1007–1014.

[14] M.A. Wimmer, A. Fischer, R. Buscher, R. Pourzal, C. Sprecher, R. Hauert, J.J. Jacobs, Wear mechanisms in metal-on-metal bearings: The importance of tribochemical reaction layers, J. Orthop. Res. 28 (2011) 436–443.

[15] M. Burgett, T. Donaldson, I.C. Clarke, C. Savisaar, J. Bowsher, Denatured protein deposits identified on simulator and explants hip bearings, in: S.M. Kurtz, A.S. Greenwald, W.M. Mihalko, J.E. Lemons (Eds.), Metal-on-Metal Total Hip Replacement Devices, ASTM International, West Conshohocken, 2013, pp. 310–322, STP 1560.

[16] Y. Yan, A. Neville, D. Dowson, S. Williams, J. Fisher, Tribofilm formation in biotribocorrosion – does it regulate ion release in metal-on-metal artificial hip joints? Proc. IMechE. Part J: J. Eng. Tribol. 224 (2010) 997–1006.

[17] J. Hesketh, M. Ward, D. Dowson, A. Neville, The composition of tribofilms produced on metal-on-metal hip bearings, Biomaterials 35 (2014) 2113–2119.

[18] Y. Liao, R. Pourzal, M.A. Wimmer, J.J. Jacobs, A. Fischer, L.D. Marks, Graphitic tribological layers in metal-on-metal hip replacements, Science 334 (2011) 1687–1690.

[19] M.A. Wimmer, M.T. Mathew, M.P. Laurent, C. Nagelli, Y. Liao, L.D. Marks, R. Pourzal, A. Fischer, J.J. Jacobs, Tribochemical reactions in metal-on-metal hip joints influence wear and corrosion, in: S.M. Kurtz, A.S. Greenwald, W.M. Mihalko, J.E. Lemons (Eds.), Metal-on-Metal Total Hip Replacement Devices, ASTM International, West Conshohocken, 2013, pp. 292–309, STP 1560.

[20] M.T. Mathew, C. Nagelli, R. Pourzal, A. Fischer, M.P. Laurent, J.J. Jacobs, M.A. Wimmer, Tribolayer formation in a metal-on-metal (MOM) hip joint: an electrochemical investigation, J. Mech. Behav. Biomed. Mater. 29 (2014) 199–212.

[21] ASTM Standard F1537:Standard Specification for Wrought Cobalt–28Chromium–6Molybdenum Alloys for Surgical Implants (UNS R31537, UNS R31538, and UNS R31539)," ASTM International, West Conshohocken, PA, 2011, http://dx.doi.org/10.1520/F1537-11.

[22] ASTM Standard G61-86: Standard Test Method for Conducting Cyclic Potentiodynamic Polarization Measurements for Localized Corrosion Susceptibility of Iron-, Nickel-, or Cobalt-Based Alloys," ASTM International, West Conshohocken, PA, 2009, http://dx.doi.org/10.1520/G0061-86R09.

[23] M.M. Stack, G.H. Abdulrahman, Mapping erosion-corrosion of carbon steel in oil exploration conditions: some new approaches to characterizing mechanisms and synergies, Tribol. Int. 43 (2010) 1268–1277.

[24] M.T. Mathew, et al., Tribocorrosion behaviour of TiC_xO_y thin films in bio-fluids, Electrochim. Acta 56 (2010) 929–937.

[25] S. Mischler, S. Debaud, D. Landolt, Wear-accelerated corrosion of passive metals in tribocorrosion systems, J. Electrochem. Soc. 145 (1998) 750–758.

[26] Y. Yan, A. Neville, D. Dowson, Understanding the role of corrosion in the degradation of metal-on-metal implants, Proc. Inst. Mech. Eng. H 220 (2006) 173–181.

[27] A.I. Muñoz, S. Mischler, Effect of the environment on wear ranking and corrosion of biomedical CoCrMo alloys, J. Mater. Sci. Mater. Med. 22 (2011) 437–450.

[28] R.A. Gil, A.I. Muñoz, Influence of the sliding velocity and the applied potential on the corrosion and wear behavior of HC CoCrMo biomedical alloy in simulated body fluids, J. Mech. Behav. Biomed. Mater. 4 (2011) 2090–2102.

[29] M.T. Mathew, M.J. Runa, M.P. Laurent, J.J. Jacobs, L.A. Rocha, M.A. Wimmer, Tribocorrosion behavior of CoCrMo alloy for hip prosthesis as a function of load: a comparison between two testing systems, Wear 271 (2011) 1210–1219.

[30] V. Swaminathan, J.L. Gilbert, Fretting corrosion of CoCrMo and Ti_6Al_4V interfaces, Biomaterials 33 (2012) 5487–5503.

[31] S. Mischler, A.I. Muñoz, Wear of CoCrMo alloys used in metal-on-metal hip joints: a tribocorrosion appraisal, Wear 297 (2013) 1081–1094.

[32] M.T. Mathew, J.J. Jacobs, M.A. Wimmer, Wear–corrosion synergism in a CoCrMo hip bearing alloy is influenced by proteins, Clin. Orthop. Relat. Res. 470 (2012) 3109–3117.

[33] E.J. Martin, R. Pourzal, M.T. Mathew, K.R. Shull, Dominant role of molybdenum in the electrochemical deposition of biological macromolecules on metallic surfaces, Langmuir 29 (2013) 4813–4822.

[34] D.A. Rigney, J.E. Hammerberg, Mechanical mixing and the development of nanocrystalline material during the sliding of metals, in: Y.W. Chung, D. C. Dunand, P. Liaw, G.B. Olson (Eds.), Advanced Materials in the 21st Century: The 1999 Julia R. Weertman Symposium, The Minerals, Metals & Materials Society, USA, 1999, pp. 465–474.

[35] A. Fischer, S. Weiß, M.A. Wimmer, The tribological difference between biomedical steels and CoCrMo-alloys, J. Mech. Behav. Biomed. Mater. 9 (2012) 50–62.

[36] Y. Yan, A. Neville, D. Dowson, Biotribocorrosion-an appraisal of the time dependence of wear and corrosion interactions: II. Surface analysis, J. Phys. D Appl. Phys. 39 (2006) 206–212.

[37] N. Beckmann, P.A. Romero, D. Linsler, M. Dienwiebel, U. Stolz, M. Moseler, P. Gumbsch, Origins of folding instabilities on polycrystalline metal surfaces, Phys. Rev. Appl. 2 (2014) 064004.

[38] M.T. Mathew, T. Uth, N.J. Hallab, R. Pourzal, A. Fischer, M.A. Wimmer, Construction of a tribocorrosion test apparatus for the hip joint: validation, test methodology and analysis, Wear 271 (2013) 2651–2659.